ARTICLE OPEN ACCESS

Early infantile epileptic-dyskinetic encephalopathy due to biallelic *PIGP* mutations

Annalisa Vetro, PhD,* Tiziana Pisano, MD,* Silvia Chiaro, MD, Elena Procopio, MD, Azzurra Guerra, MD, Elena Parrini, PhD, Davide Mei, MSc, Simona Virdò, MSc, Giusi Mangone, MSc, Chiara Azzari, MD, PhD, and Renzo Guerrini, MD, FRCP

Correspondence
Dr. Guerrini
r.guerrini@meyer.it

Neurol Genet 2020;6:e387. doi:10.1212/NXG.0000000000000387

Abstract

Objective

To describe clinical, biochemical, and molecular genetic findings in a large inbred family in which 4 children with a severe early-onset epileptic-dyskinetic encephalopathy, with suppression burst EEG, harbored homozygous mutations of phosphatidylinositol glycan anchor biosynthesis, class P (*PIGP*), a member of the large glycosylphosphatidylinositol (GPI) anchor biosynthesis gene family.

Methods

We studied clinical features, EEG, brain MRI scans, whole-exome sequencing (WES), and measured the expression of a subset of GPI-anchored proteins (GPI-APs) in circulating granulocytes using flow cytometry.

Results

The 4 affected children exhibited a severe neurodevelopmental disorder featuring severe hypotonia with early dyskinesia progressing to quadriplegia, associated with infantile spasms, focal, tonic, and tonic-clonic seizures and a burst suppression EEG pattern. Two of the children died prematurely between age 2 and 12 years; the remaining 2 children are aged 2 years 7 months and 7 years 4 months. The homozygous c.384del variant of *PIGP*, present in the 4 patients, introduces a frame shift 6 codons before the expected stop signal and is predicted to result in the synthesis of a protein longer than the wild type, with impaired functionality. We demonstrated a reduced expression of the GPI-AP CD16 in the granulocytic membrane in affected individuals.

Conclusions

PIGP mutations are consistently associated with an epileptic-dyskinetic encephalopathy with the features of early infantile epileptic encephalopathy with profound disability and premature death. CD16 is a valuable marker to support a genetic diagnosis of inherited GPI deficiencies.

*These authors contributed equally to the manuscript.

From the Pediatric Neurology (A.V., T.P., S.C., E. Parrini, D.M., S.V., R.G.), Neurogenetics and Neurobiology Unit and Laboratories, Meyer Children's Hospital, University of Florence; Metabolic and Muscular Unit (E. Procopio), Meyer Children's Hospital, University of Florence; Department of Medical and Surgical Science (A.G.), University of Modena and Reggio Emilia; Pediatric Immunology (G.M., C.A.), Department of Health Sciences, Meyer Children's Hospital, University of Florence; and IRCCS Stella Maris (R.G.), Pisa, Italy.

Go to Neurology.org/NG for full disclosures. Funding information is provided at the end of the article.

The Article Processing Charge was funded by Università di Firenze—Dip. Neurofarba.

Glossary

EIEE = early infantile epileptic encephalopathy; **ER** = endoplasmic reticulum; **FLAER** = fluorescein-labeled proaerolysin; **GnomAD** = Genome Aggregation Database; **GPI** = glycosylphosphatidylinositol; **GPI-APs** = glycosylphosphatidylinositol-anchored proteins; **IGD** = inherited GPI deficiency; **InDels** = insertion/deletions; **MFI** = median fluorescence intensity; **MIM** = Mendelian Inheritance in Man; ***PIGP*** = phosphatidylinositol glycan anchor biosynthesis, class P; **ROH** = regions of homozygosity; **SSC** = side scattered.

Glycosylphosphatidylinositol-anchored proteins (GPI-APs) represent a heterogeneous group of cell surface proteins tethered to the cell membrane by the post-translational addition of a GPI to the C-terminus. More than 150 GPI-APs have been identified in multiple biological contexts,[1] often playing a role in CNS development and synaptic function and plasticity.[2] The GPI-anchor precursors are synthesized in the endoplasmic reticulum (ER) and then attached to target proteins, which are further remodeled both in the ER and in the Golgi complex before to be exposed on the cell surface.[3] Mutations in at least 19 genes involved in this multistep pathway have been associated with a relatively novel group of disorders known as inherited GPI deficiencies[4] (IGDs; table e-1, links.lww.com/NXG/A204) all transmitted in an autosomal recessive manner, with the exception of those associated with mutations of *PIGA*, which are X-linked recessive.[5] The associated phenotype is variable, with global developmental delay, hypotonia, and epilepsy as the most consistent findings. A ~0.15% incidence of IGDs in patients with developmental delay has been reported in the large Deciphering Developmental Disorders study cohort.[6] Phosphatidylinositol glycan anchor biosynthesis, class P (*PIGP*) has only recently been linked to human diseases,[7] through the description of 2 siblings with early infantile epileptic encephalopathy (EIEE 55, Mendelian Inheritance in Man [MIM] #617599) and compound heterozygous mutations of the gene. We describe 2 pairs of siblings with EIEE, dyskinetic movements, and profound developmental delay, born to consanguineous parents in a large inbred family, in whom we identified a c.384del homozygous variant in the *PIGP* gene (accession number NM_153682.2).

Methods

The family was ascertained through the proband (figure 1), referred to our Pediatric Neurology Unit for clinical and diagnostic purposes. Seizure types were classified according to the 2017 International League Against Epilepsy classification.[8]

Standard protocol approvals, registrations, and patient consents

We obtained written informed consent to disclose clinical information, neuroimaging, and molecular investigations. The study was approved by the Pediatric Ethics Committee of the Tuscany Region, in the context of the DESIRE project (Seventh Framework Programme FP7; grant agreement no. 602531).

Genetic investigations

We performed whole-exome sequencing (WES) on DNA from patient 1 (V-3 in figure 1) and his parents using the SureSelectXT Clinical Research Exome kit (Agilent Technologies, Santa Clara, CA) for library preparation and target enrichment. We sequenced the captured DNA libraries by a paired-end 2 × 150 bp protocol on the NextSeq500 (Illumina, San Diego, CA) to obtain an average coverage of above 110×, with 97.6% of target bases covered at least 10×. We aligned the sequencing reads to the GRCh37/hg19 human genome reference assembly by the BWA software package and used the GATK suite for base quality score recalibration,[9] realignment of insertion/deletions (InDels), and variant calling, according to GATK Best Practices recommendations.[10] For the annotation and filtering of exonic/splice site single nucleotide variants (SNVs) and coding InDels, we used VarSeq software (Golden Helix, Inc v1.4.6, Bozeman, MT), focusing on variants with minor allele frequency lower than 0.01 in the Genome Aggregation Database (GnomAD v2.1, gnomad.broadinstitute.org/). We further excluded population-specific variants by interrogating our internal database (WES data from more than 900 patients with developmental and epileptic encephalopathy and 200 healthy parents) and evaluated the potential functional impact of SNVs and InDels by the precomputed genomic variants score from database for nonsynonymous SNPs' functional predictions,[11] which was integrated in the annotation pipeline. We also manually interrogated in silico prediction tools.[12–15] Separately, we evaluated possible regions of autozygosity by Agile VCF Mapper software (dna.leeds.ac.uk/autozygosity/). For selected variants, we visually inspected the quality of reads alignment using the Integrative Genomics Viewer (IGV v2.4)[16] and then proceeded to validation and segregation analysis by Sanger sequencing (primers and conditions available on request). Pathogenic variants were submitted to the Leiden Open Variation Database version 3.0.

Flow cytometry analysis of GPI-APs

We performed flow cytometry analysis on 100 μL of fresh blood from patients 2 and 4 and 10 healthy age-matched controls. We lysed the red blood cells in FACS Lysing Solution (BD Biosciences, Franklin Lakes, NJ) and stained all the samples with the following fluorescent antibodies: CD45 PerCP-Cy 5.5, CD55 PE, CD59 FITC, CD16 PE, CD24 PE (all from BD Biosciences), and with fluorescein-labeled proaerolysin (FLAER)-Alexa Fluor488 (Cedarlane, Burlington, ON, Canada), in accordance with manufacturers'

Figure 1 Pedigree of the family with *PIGP* c.384del homozygous variant

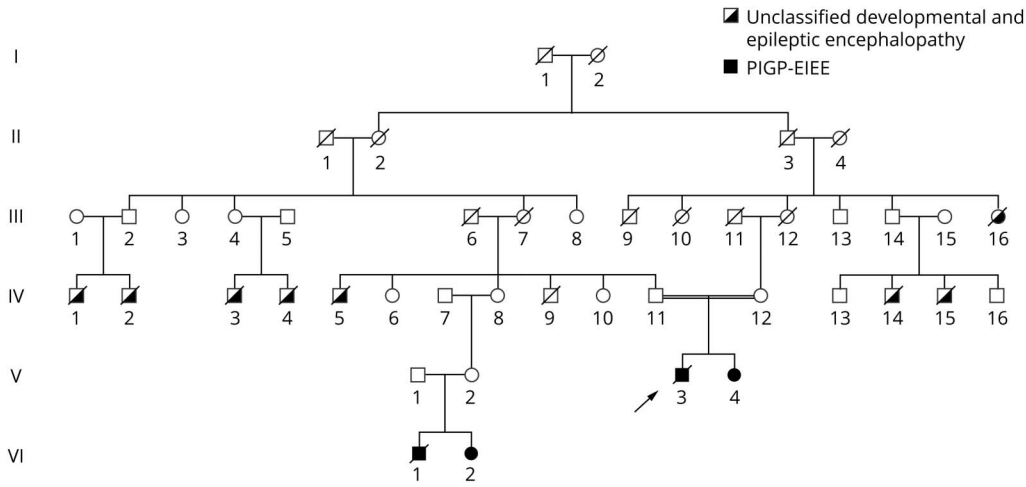

The arrow points to the proband (patient 1). Individuals with a history of seizures and global developmental delay, but insufficient information to identify a specific phenotype, are designated as "unclassified developmental and epileptic encephalopathy."

instructions. We acquired the data by BD FACS Canto II Flow Cytometer and FACSDIVA software (BD Biosciences) and identified white blood cells by side scattered light (SSC) and forward scattered light. We selected granulocytes as granular (SSC-A high) and CD45-positive cells. For each marker, we measured the median fluorescence intensity (MFI) and calculated the ratio of patients' MFI vs the average MFI of controls. We used the Student *t* test to assess statistical significance of the MFI observations.

Data availability

All the data from this study are available from the corresponding author on reasonable request.

Results

Clinical findings

Clinical findings are summarized in table 1. A family history of seizures and neonatal or child mortality was reported in both parental lines. In figure 1 individuals with a history of seizures and global developmental delay, but insufficient information to identify a specific phenotype, were designated as "unclassified developmental and epileptic encephalopathy."

Patient 1 (V-3, figure 1) was the first child born to a healthy consanguineous couple (second cousins). The boy was born at 39 weeks of gestation by Caesarian section because of nuchal cord. Prenatal history was unremarkable. Head circumference (OFC) at birth was 35 cm (50th centile), weight 3.650 kg (50–85th centile), and length 50.5 cm (50th centile). Apgar scores were 7-5-8. No dysmorphic features were noticed. From the first months of life, the boy manifested ocular and limb dyskinesia, later progressing to spastic quadriplegia. At age 3 months, severe developmental delay, epileptic encephalopathy with focal seizures, epileptic spasms, and generalized tonic or clonic seizures became apparent. Seizures had a daily frequency and were aggravated by fever or infections. EEGs showed an asymmetric burst suppression pattern (figure 2A). Brain MRI at 3 months showed mildly reduced white matter bulk with thin corpus callosum, ventriculomegaly, and dilated frontotemporal subarachnoid space. After ab ingestis pneumonia, percutaneous endoscopic gastrostomy was performed at age 7 months. Recurrent respiratory infections prompted frequent hospitalizations with oxygen therapy or continuous positive airway pressure support. Several combinations of antiepileptic drugs (including valproate, phenobarbital, phenytoin, topiramate, carbamazepine, vigabatrin, levetiracetam, rufinamide, clonazepam, and lorazepam) failed to control seizures. Over the years, the patient experienced frequent episodes of status epilepticus that were successfully treated with high doses of benzodiazepines or phenytoin. Follow-up brain MRI scans at 18 and 30 months confirmed the initial findings (figure 3, A–C). At the last clinical evaluation (12 years), the patient exhibited acquired microcephaly (OFC 50 cm, −2 SD), an unclassifiable form of epileptic encephalopathy with asymmetric burst suppression, and spastic quadriplegia. The child died at age 12 years due to respiratory infection.

Plasma metabolic workout and CSF lactate, amino acids, and neurotransmitters were unremarkable. Serum alkaline phosphatase levels were normal. Karyotype, DNA methylation analysis for Angelman syndrome, array comparative genomic hybridization (aCGH), and next-generation sequencing analysis of a panel of 95 genes associated with epilepsy were all unrevealing. Muscle biopsy showed reduced complex I activity (citrate synthase reduced by 47% with respect to reference value) and pyruvate dehydrogenase complex (PDC) activity (63.3% reduction). Reduced PDC was also present in cultured skin fibroblasts (69.5% reduction).

Table 1 Summary of the clinical features in our patients 1–4

Patient	1	2	3	4
Sex	M	F	M	F
Age at last evaluation	12 y (deceased)	25 mo	27 mo (deceased)	6 y 5 mo
Auxologic parameters at birth	OFC 35 cm (50th centile), weight 3.650 kg (50–85th centile), and length 50.5 cm (50th centile)	OFC 34 cm (50th centile), weight 2.800 kg (15–25th centile), and length 47 cm (25th centile)	OFC 35 cm (50th centile), weight 3.300 kg (50th centile), and length 51 cm (50th centile)	OFC 35 cm (50th centile), weight 3.300 kg (75th centile), and length 50 cm (50th centile)
Age at seizure onset/type	3 mo; focal, spasms, GTC	3 mo; focal, spasms, GTC	3 mo; focal	3 mo; focal, spasms
EEG	Multifocal discharges and asymmetric BS	Multifocal discharges and asymmetric BS	Multifocal discharges and BS	Multifocal discharges
Brain MRI	Mildly reduced white matter volume, thin corpus callosum, ventriculomegaly, and dilated frontotemporal subarachnoid space	Mildly reduced white matter volume, thin corpus callosum, and dilated frontotemporal subarachnoid space	Diffuse brain atrophy, diffuse white matter high signal intensity, and hypoplasia of the corpus callosum	Severe atrophy of the right hemisphere
Age at onset/ movement disorder	1 mo; ocular and limb dyskinesia, then spastic quadriplegia	3 mo; dyskinesia mainly involving the face, eyes, and limbs	8 mo; poor motor pattern with dyskinesia	3 mo; dyskinesia of the limbs, then spastic quadriplegia
Other neurologic features	Axial hypotonia and DD	Axial hypotonia and DD	Axial hypotonia and DD	DD
AEDs	VPA, PB, PHT, PB, TPM, CBZ, VGB, LEV, RUF, CNZ, LZP, and KD	PB, LEV, TPM, CNZ, and hydrocortisone	PB, CBZ, and CNZ	PHT, LEV, TPM, ACTH, CBZ, CLB, and KD
PEG	Yes	No	No	Yes

Abbreviations: ACTH = adrenocorticotropic hormone; AED = antiepileptic drug; BS = burst suppression; CBZ = carbamazepine; CLB = clobazam; CNZ = clonazepam; DD = developmental delay; GTC = generalized tonic-clonic seizure; OFC = head circumference; KD = ketogenic diet; LEV = levetiracetam; LZP = lorazepam; mo = months; PB = phenobarbital; PEG = percutaneous endoscopic gastrostomy; PHT = phenytoin; RUF = rufinamide; TPM = topiramate; VGB = vigabatrin; VPA = valproate; y = years.

Patient 2 (V-4, figure 1) was the sister of patient 1. Her pre- and peri-natal history was unremarkable. Early normal development was reported up to age 3 months, when poor visual fixation, axial hypotonia and dyskinetic movements, mainly involving the orobuccal area, eyes and limbs, were noticed and tonic axial and focal seizures appeared. At 8 months, infantile spasms became apparent. Interictal EEG at 4 months revealed multifocal epileptiform activity with an asymmetric burst suppression pattern (figure 2, B and C). Her brain MRI showed mildly reduced white matter volume, thin corpus callosum, and frontotemporal subarachnoid space enlargement (figure 3, D–F). Topiramate (5 mg/kg/die) transiently reduced seizures frequency. Global development never progressed beyond a 3-month-old level. Her medical history was also notable for recurrent respiratory infections and dysphagia.

At last clinical evaluation (25 months), the patient had an OFC of 50 cm (15th centile) and exhibited an unclassifiable epileptic encephalopathy with asymmetric suppression bursts and dyskinetic movements, closely resembling the clinical picture observed in her brother at the same age. Plasma metabolic workout was unremarkable.

Patient 3 (VI-1, figure 1) was the second cousin of patients 1 and 2. His developmental milestones were delayed. At age 3 months, he had no social smiling, could not visually fix or track, and manifested daily focal seizures with a burst suppression EEG pattern (figure 2D). Brain MRI at 7 months revealed diffuse atrophy, with frontal lobe predominance, diffuse high signal intensity in the white matter, and thin corpus callosum (figure 3, G–I). Clinical examination at 8 months showed deceleration in head growth (OFC 45 cm and 15th centile), axial hypotonia, limb hypertonus, and a poor motor pattern with dyskinetic movements. Plasma metabolic workout was unremarkable. This boy died of sepsis when he was aged 2 years 3 months.

Patient 4 (VI-2, figure 1) was the sister of patient 3. At age 3 months, dyskinetic movements were noticed and a seizure disorder appeared, soon becoming a severe epileptic encephalopathy. The movement disorder progressively translated into severe spastic quadriplegia.

Brain MRI at 9 months showed diffuse cerebral atrophy, increased white matter signal intensity, and thin corpus callosum. A follow-up MRI at age 3 years revealed brain asymmetry with severe atrophy of the right hemisphere (figure 3, J–L). At last clinical evaluation, at age 6 years and 5 months, the clinical picture was unchanged.

Plasma metabolic workout was unremarkable. The PDC activity assay in cultured fibroblasts was normal. Genetic

Figure 2 EEGs of patients 1–3

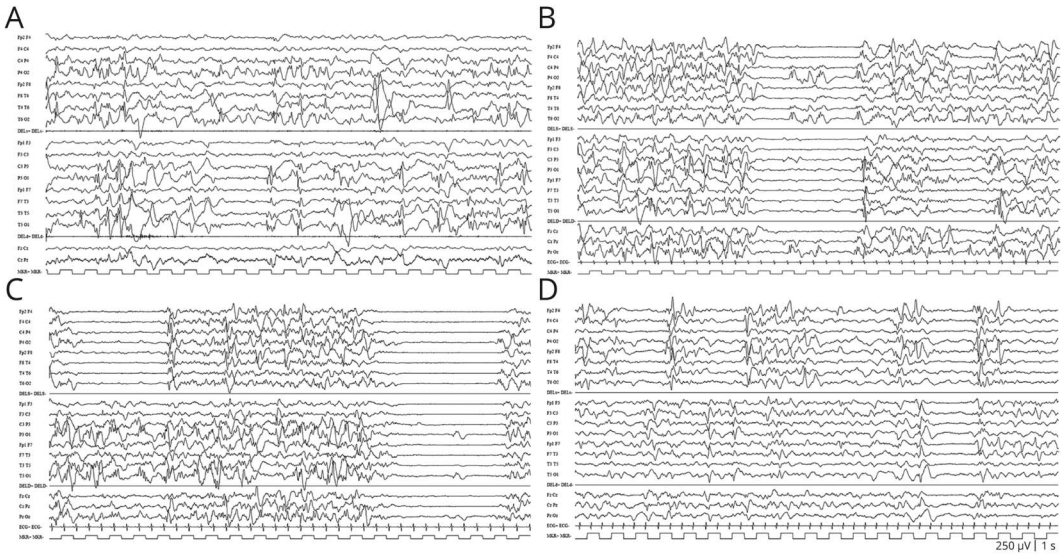

(A) Patient 1: EEGs exhibiting multifocal discharges with asymmetric burst suppression (BS) at age 7 months. (B–C) Patient 2: asymmetric BS at age 3 months. (D) Patient 3: asymmetric BS at age 5 months.

investigations including aCGH and Sanger sequencing of single genes (*ARX*, *CDKL5*, *KCNQ2*, *POLG*, and *STXBP1*) were unrevealing.

Genetic investigations

Trio-WES analysis highlighted in the DNA of patient 1 multiple large homozygous segments (regions of homozygosity, ROH) involving different chromosomes, as to be expected considering parental consanguinity. We calculated the total length of ROH larger than 5 Mb (101 Mb) to estimate the percentage of homozygosity (F_{ROH}) and found it to be ≈3.7%, which was higher than expected for a fifth degree of relationship.[17] As the family came from a small isolated town, this was probably the result of unknown background relatedness. According to the family history, we focused on a recessive mode of inheritance, narrowing the number of candidate variants to 3, which were all homozygous in patient 1 (*WDR43,* NM_015131.2:c.349C>T; *LTBP2,* NM_000428.2:c.5155G>A; *PIGP,* NM_153682.2:c.384del). The *PIGP* c.384del variant was located in a large ROH spanning ≈11.9 Mb of chromosome 21 (hg19, chr21:34157235-46047925) and after segregation analysis resulted to be the only homozygous variant shared by all patients (figure 4, A and B). The parents of patients 1–2 and 3–4 were heterozygous carriers. According to the GnomAD database (v2.1), the global allele frequency of the variant was 3×10^{-5}. The c.384del introduced a frame shift 6 codons before the expected stop signal [p.(Glu129Asnfs*34)]. We excluded pathogenic/likely pathogenic variants in genes associated with PDC deficiency (*PDHB*, *LIAS*, *PDP1*, *PDHX*, *DLAT*, *PDHA1*; MIM: PS312170), all of which were well covered by WES data. None of these genes were in one of the ROHs. The *LTBP2* c.5155G>A variant [p.(Val1719Met)], homozygous in the DNA of patient 1, was not previously reported and was indicated as "tolerated" by in silico prediction tools. As defects of the *LTBP2* gene are associated with primary congenital glaucoma (MIM #602091), we considered this variant as an incidental finding.

Flow cytometry analysis of GPI-APs

To determine the effect of the *PIGP* gene variant on the surface expression of GPI-APs, we measured, by flow cytometry, the MFI of CD16, CD24, CD55, CD59, and FLAER in granulocytes of patients 2 and 4 and in 10 age-matched controls (table e-2, links.lww.com/NXG/A204). We observed a significant reduction of CD16 of approximately 40% ($p < 0.05$) and 56% ($p < 0.01$) in patients 2 and 4, respectively (figure 4, C and D). In patient 4, we also observed a reduced signal of CD24 (−45%, figure 4D) that did not reach statistical significance. No differences were noticeable for the CD55, CD59, and FLAER markers (table e-2).

Discussion

IGDs are a relatively novel clinical entity. Their recognition is often challenging, as the main features, which include developmental delay, abnormal movements, and epilepsy, are common to many neurodevelopmental disorders. In the large consanguineous family we describe, 2 pairs of affected siblings carried a c.384del homozygous *PIGP* variant and manifested a form of EIEE featuring infantile spasms, focal, tonic, and tonic-clonic seizures and an EEG pattern associating burst suppression and multifocal discharges. In addition to the devastating epilepsy, patients exhibited severe developmental delay, hypotonia, and dyskinesia, evolving to spastic quadriplegia.

Figure 3 Brain MRI summarizing the main features in 4 patients

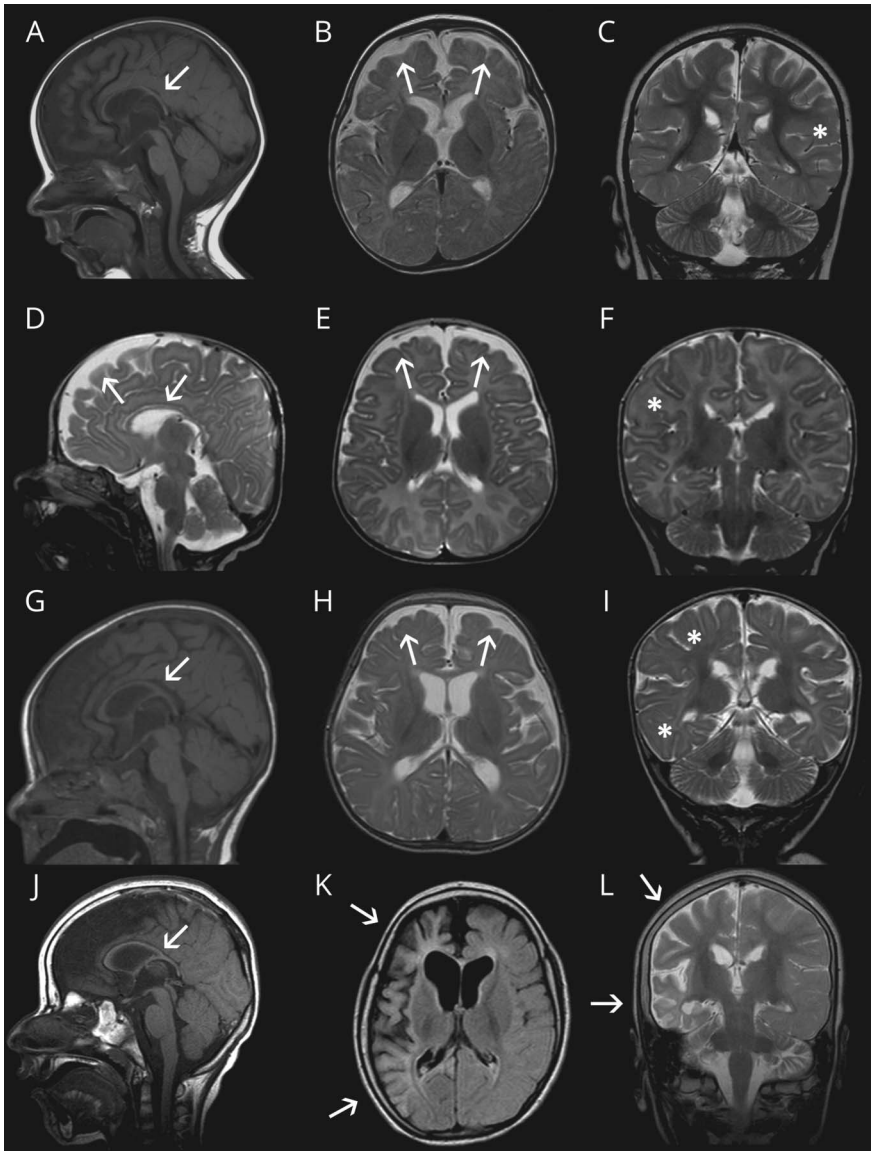

Patient 1 (18 months): (A) sagittal T1-weighted (W), (B) axial T2-W, and (C) coronal T2-W images. There is mildly reduced white matter volume (asterisk), thin corpus callosum, ventriculomegaly, and enlarged subarachnoid space in the frontotemporal areas (arrows). Patient 2 (3 months): (D–F) sagittal, axial, and coronal T2-W images. Mildly reduced white matter volume (asterisk), thin corpus callosum, and enlarged subarachnoid space in the frontotemporal areas (arrows). Patient 3 (7 months): (G) sagittal T1-W, (H) axial T2-W, and (I) coronal T2-W. Diffuse cerebral atrophy (arrows), particularly affecting the frontal lobes, diffusely increased white matter intensity (asterisk) and hypoplasia of the corpus callosum (arrow). Patient 4 (3 years): (J) sagittal T1-W, (K) axial flair, and (L) coronal T2-W. Brain asymmetry due to severe atrophy of the right hemisphere with ventriculomegaly and thin corpus callosum.

Biallelic defects of *PIGP* have previously been reported in 2 siblings[7] and in a further unrelated girl with EIEE.[18] Additional clinical features we observed in the patients we describe here include the dyskinetic movement disorder. Dyskinetic movements have been reported in a subset of patients with mutations of *PIGA*, *PIGN*, *PGAP1*, and *PGAP3*[19–22] but do not appear as a frequent finding in IGDs, according to the GPI biosynthesis disorder database.[23] In our patients, dyskinetic movements became apparent in the first months of life and progressed to spastic quadriplegia since the third year of life in the 2 patients who grew older than that age (patients 1 and 4).

In patient 1, a mitochondrial disorder was clinically suspected and partially supported by reduced complex I activity in the muscle and reduced PDC activity both in muscle and in cultured fibroblasts. However, the PDC dosage in fibroblasts of patient 4 was normal. PDC deficiency in patient 1 was likely a secondary unspecific feature associated with the *PIGP* genetic defect. Nonspecific mitochondrial dysfunctions have been reported in some patients with *PIGA* and *PIGG* mutations,[24,25] although the mechanism underlying this phenomenon remains unclear.

The homozygous c.384del we identified (previously reported as c.456del according to the NM_153681.2 isoform) had also been identified, again in homozygosity, in a Polish girl born from nonconsanguineous parents, with developmental and epileptic encephalopathy.[18] The same variant had also been reported in compound heterozygosity with the start loss c.2T>C [p.(Met1Thr)] in 2 siblings of French-Irish ancestry with EIEE, hypotonia, and profound developmental delay.[7] The c.384del variant has 9 alleles in the GnomAD database (global allele

Figure 4 Genetic and flow cytometry investigations

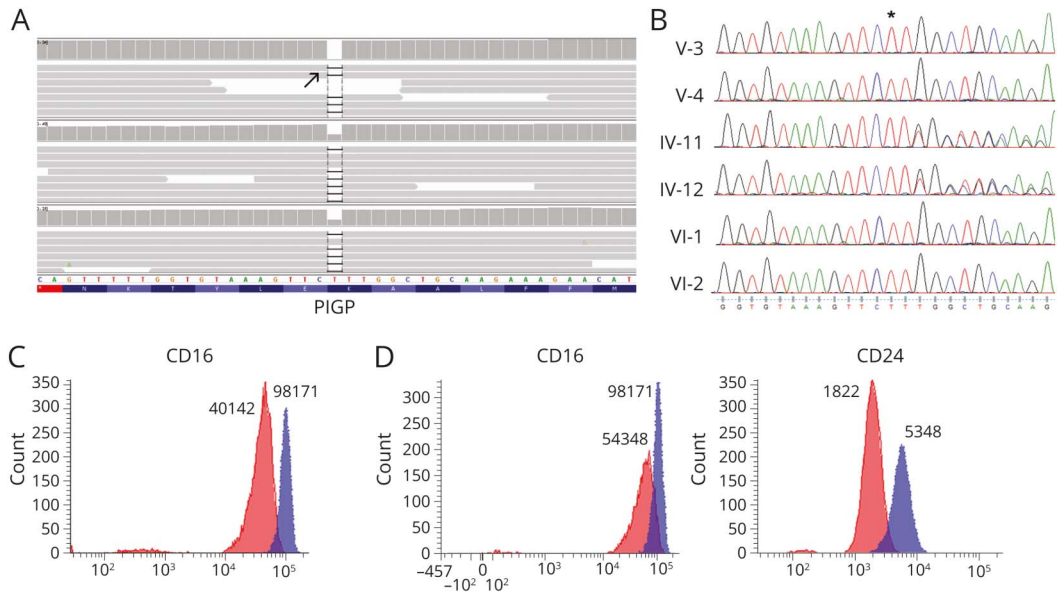

(A) Screenshot of a 40-bp window (chr21:38437883-38437923, hg19) including the c.384del variant of *PIGP* as visualized by Integrative Genomics Viewer (IGV v2.3).[16] Gray bars represent the mapped reads aligned to the reference genome, whose sequence is shown below. The upper panel shows the homozygous single T base deletion at chr21:38437903 (arrow) in patient 1, which is heterozygous in both parents (middle and lower panels). A coverage track is displayed above each panel. (B) Sanger sequencing: all affected individuals are homozygous for the c.384del. Both parents of patients 1 and 2 are heterozygous carriers. The position of the deleted base is indicated by the asterisk in the upper panel. The reference sequence is shown at the bottom of the picture. (C–D) Decreased cell surface expression of GPI-AP markers in granulocytes of patients 2 (C, red) and 4 (D, red) compared with a representative control (blue). Numbers above each histogram represent the median fluorescence intensity (MFI). CD16 is reduced in both patients. The expression of CD24 is reduced in patient 4 only. GPI-AP = GPI-anchored protein; MFI = median fluorescence intensity.

frequency 3×10^{-5}), all identified in individuals of European ancestry, suggesting a founder effect in the European population.

In patient 1, we could demonstrate that the homozygous c.384del variant of *PIGP* located in a large ROH, as expected considering the known parental consanguinity. The single base deletion introduces a frame shift 6 codons before the expected stop signal and is predicted to result in the synthesis of a protein longer than the wild type (27 additional amino acids, p.[Glu129Asnfs*34]). The reduced expression and impaired functionality of the aberrant protein has been documented.[7] A decreased cell surface presentation of GPI-APs in blood cells and fibroblasts of patients with IGDs is considered a hallmark of the disease, although a certain variability is observed, depending on the cell type and the investigated marker, even in patients with mutations of the same gene.[26]

There is no standardized method for the immunophenotypic analysis of blood cells in IGDs, although most flow cytometric analyses have been performed on granulocytes with the markers CD16, CD55, CD59, CD24, CD73, and FLAER.[26,27] Johnstone et al.[7] showed a reduction in the expression of FLAER-labeled GPI, CD16, and CD55 in 1 patient with *PIGP* defects. We investigated the surface expression of FLAER-labeled GPI, and of a subset of GPI-APs in circulating granulocytes of the 2 surviving patients (2 and 4), compared with a group of 10 age-matched healthy controls and found significantly reduced CD16 in both patients. CD24 was reduced in patient 4 only, whereas we could not observe relevant differences in the remaining markers.

The reduced expression of CD16 in granulocytes is considered a reliable indicator of impaired GPI synthesis in paroxysmal nocturnal hemoglobinuria, a separate non-neurologic GPI deficiency associated with somatic mutations of *PIGA* (MIM: #300818).[28] In patients with IGD due to *PIGC* mutations, only CD16 showed a significant and constant decrease in granulocytes, whereas other markers, including CD55, CD59, and FLAER, showed fluctuating variations.[29] We suggest to test CD16 as a marker to support the interpretation of variants of unknown significance in genes involved in the GPI biosynthesis and remodeling pathway. In patients with IGDs, serum transferrin isoelectric focusing is normal and no other laboratory markers are available to support the clinical suspect and the genetic diagnosis.

Study funding

Supported by DESIRE project, Seventh Framework Programme FP, grant agreement no. 602531 to RG.

Disclosure

Disclosures available: Neurology.org/NG.

Publication history

Received by *Neurology: Genetics* July 24, 2019. Accepted in final form October 28, 2019.

Appendix Authors

Name	Location	Role	Contribution
Annalisa Vetro, PhD	Meyer Children's Hospital, University of Florence, Italy	Author	Study design, acquisition and interpretation of data, and manuscript drafting
Tiziana Pisano, MD	Meyer Children's Hospital, University of Florence, Italy	Author	Study design, acquisition and interpretation of data, and manuscript drafting
Silvia Chiaro, MD	Meyer Children's Hospital, University of Florence, Italy	Author	Acquisition of clinical data and follow-up of the patients
Elena Procopio, MD	Meyer Children's Hospital, University of Florence, Italy	Author	Acquisition of clinical data and follow-up of the patients
Azzurra Guerra, MD	University of Modena and Reggio Emilia, Italy	Author	Acquisition of clinical data and follow-up of the patients
Elena Parrini, PhD	Meyer Children's Hospital, University of Florence, Italy	Author	Acquisition of genetic data
Davide Mei, MSc	Meyer Children's Hospital, University of Florence, Italy	Author	Acquisition of genetic data
Simona Virdò, MSc	Meyer Children's Hospital, University of Florence, Italy	Author	Acquisition of genetic data
Giusi Mangone, MSc	Meyer Children's Hospital, University of Florence, Italy	Author	Acquisition and interpretation of flow cytometry data and manuscript drafting
Chiara Azzari, MD, PhD	Meyer Children's Hospital, University of Florence, Italy	Author	Flow cytometry data interpretation and critical revision
Renzo Guerrini, MD, FRCP	Meyer Children's Hospital, University of Florence, Italy; IRCCS Stella Maris, Pisa, Italy	Author	Study supervision and concept and critical revision of the manuscript for intellectual content

References

1. Kinoshita T, Fujita M. Biosynthesis of GPI-anchored proteins: special emphasis on GPI lipid remodeling. J Lipid Res 2016;57:6–24.
2. Um JW, Ko J. Neural glycosylphosphatidylinositol-anchored proteins in synaptic specification. Trends Cell Biol 2017;27:931–945.
3. Kinoshita T. Biosynthesis and deficiencies of glycosylphosphatidylinositol. Proc Jpn Acad Ser B 2014;90:130–143.
4. Bellai-Dussault K, Nguyen TTM, Baratang NV, Jimenez-Cruz DA, Campeau PM. Clinical variability in inherited glycosylphosphatidylinositol deficiency disorders. Clin Genet 2019;95:112–121.
5. Johnston JJ, Gropman AL, Sapp JC, et al. The phenotype of a germline mutation in PIGA: the gene somatically mutated in paroxysmal nocturnal hemoglobinuria. Am J Hum Genet 2012;90:295–300.
6. Pagnamenta AT, Murakami Y, Taylor JM, et al. Analysis of exome data for 4293 trios suggests GPI-anchor biogenesis defects are a rare cause of developmental disorders. Eur J Hum Genet 2017;25:669–679.
7. Johnstone DL, Nguyen TTM, Murakami Y, et al. Compound heterozygous mutations in the gene PIGP are associated with early infantile epileptic encephalopathy. Hum Mol Genet 2017;26:1706–1715.
8. Scheffer IE, Berkovic S, Capovilla G, et al. ILAE classification of the epilepsies: position paper of the ILAE commission for classification and terminology. Epilepsia 2017;58:512–521.
9. Li H, Durbin R. Fast and accurate short read alignment with Burrows-Wheeler transform. Bioinformatics 2009;25:1754–1760.
10. DePristo MA, Banks E, Poplin R, et al. A framework for variation discovery and genotyping using next-generation DNA sequencing data. Nat Genet 2011;43:491–498.
11. Liu X, Jian X, Boerwinkle E. dbNSFP: a lightweight database of human nonsynonymous SNPs and their functional predictions. Hum Mutat 2011;32:894–899.
12. Adzhubei IA, Schmidt S, Peshkin L, et al. A method and server for predicting damaging missense mutations. Nat Methods 2010;7:248–249.
13. Schwarz JM, Rödelsperger C, Schuelke M, Seelow D. MutationTaster evaluates disease-causing potential of sequence alterations. Nat Methods 2010;7:575–576.
14. Kumar P, Henikoff S, Ng PC. Predicting the effects of coding non-synonymous variants on protein function using the SIFT algorithm. Nat Protoc 2009;4:1073–1081.
15. Rentzsch P, Witten D, Cooper GM, Shendure J, Kircher M. CADD: predicting the deleteriousness of variants throughout the human genome. Nucleic Acids Res 2019;47:D886–D894.
16. Thorvaldsdóttir H, Robinson JT, Mesirov JP. Integrative Genomics Viewer (IGV): high-performance genomics data visualization and exploration. Brief Bioinform 2013;14:178–192.
17. Sund KL, Rehder CW. Detection and reporting of homozygosity associated with consanguinity in the clinical laboratory. Hum Hered 2014;77:217–224.
18. Krenn M, Knaus A, Westphal DS, et al. Biallelic mutations in PIGP cause developmental and epileptic encephalopathy. Ann Clin Transl Neurol 2019;6:968–973.
19. Howard MF, Murakami Y, Pagnamenta AT, et al. Mutations in PGAP3 impair GPI-anchor maturation, causing a subtype of hyperphosphatasia with mental retardation. Am J Hum Genet 2014;94:278–287.
20. Swoboda KJ, Margraf RL, Carey JC, et al. A novel germline PIGA mutation in Ferro-Cerebro-Cutaneous syndrome: a neurodegenerative X-linked epileptic encephalopathy with systemic iron-overload. Am J Med Genet A 2014;164A:17–28.
21. Maydan G, Noyman I, Har-Zahav A, et al. Multiple congenital anomalies-hypotonia-seizures syndrome is caused by a mutation in PIGN. J Med Genet 2011;48:383–389.
22. Kettwig M, Elpeleg O, Wegener E, et al. Compound heterozygous variants in PGAP1 causing severe psychomotor retardation, brain atrophy, recurrent apneas and delayed myelination: a case report and literature review. BMC Neurol 2016;16:74.
23. Baratang NV, Jimenez Cruz DA, Ajeawung NF, Nguyen TTM, Pacheco-Cuéllar G, Campeau PM. Inherited glycophosphatidylinositol deficiency variant database and analysis of pathogenic variants. Mol Genet Genomic Med 2019;7:e00743.
24. Lionel AC, Costain G, Monfared N, et al. Improved diagnostic yield compared with targeted gene sequencing panels suggests a role for whole-genome sequencing as a first-tier genetic test. Genet Med 2018;20:435–443.
25. Tarailo-Graovac M, Sinclair G, Stockler-Ipsiroglu S, et al. The genotypic and phenotypic spectrum of PIGA deficiency. Orphanet J Rare Dis 2015;10:23.
26. Knaus A, Pantel JT, Pendziwiat M, et al. Characterization of glycosylphosphatidylinositol biosynthesis defects by clinical features, flow cytometry, and automated image analysis. Genome Med 2018;10:1–13.
27. Kato M, Saitsu H, Murakami Y, et al. PIGA mutations cause early-onset epileptic encephalopathies and distinctive features. Neurology 2014;82:1587–1596.
28. Richards SJ, Barnett D. The role of flow cytometry in the diagnosis of paroxysmal nocturnal hemoglobinuria in the clinical laboratory. Clin Lab Med 2007;27:577–590.
29. Edvardson S, Murakami Y, Nguyen TTM, et al. Mutations in the phosphatidylinositol glycan C (PIGC) gene are associated with epilepsy and intellectual disability. J Med Genet 2017;54:196–201.

Early infantile epileptic-dyskinetic encephalopathy due to biallelic *PIGP* mutations

Annalisa Vetro, Tiziana Pisano, Silvia Chiaro, et al.

Neurol Genet 2020;6;
DOI 10.1212/NXG.0000000000000387